Check for updates

SERS as a probe for the charge-transfer process in a coupled semiconductor nanoparticle system TiO₂/MBA/PbS†

Xiaolei Zhang,[ab] Lin Guo,[a] Peng Li,[a] Bing Zhao [ID] *[a] and Bo Cui[b]

A coupled semiconductor nanoparticle system composed of TiO₂ NPs, 4-mercaptobenzoic acid (4-MBA) molecules and PbS NPs has been fabricated as a model to study the involved charge transfer (CT) effect using a Surface-Enhanced Raman Scattering (SERS) technique. In this TiO₂/MBA/PbS system, the MBA molecules function as both a linker between TiO₂ and PbS NPs and a SERS probe to reveal the CT process. For the SERS enhancement behaviors of the CT-sensitive vibrational mode in 4-MBA and the Raman spectra of the phonon vibrational mode in TiO₂ NPs, there are some evident changes after adding PbS to the TiO₂/MBA system. These changes are due to the interaction between TiO₂ NPs and PbS NPs. We found that these differences, closely related to the natures of TiO₂ and PbS NPs, are a reflection of the enhanced TiO₂-to-molecule CT process in SERS. The SERS spectra of the TiO₂/MBA/CdS system were also investigated and the result is in good accordance with our theory. This work will not only help in constructing nanoscale models to study interfacial CT processes but also be of considerable value for practical application of SERS technology.

Introduction

Coupled semiconductor nanoparticle systems have been the subject of numerous investigations in recent years; the origin of the extensive interest is that coupled semiconductor nanoparticle systems exhibit a wide range of novel photoelectric properties that are finding application in solar cells, photocatalysis, supercapacitors and other power conversation devices. However, for many coupled semiconductor nanoparticle systems, the understanding of the interparticle CT processes between different semiconductor particles are still unclear, which is vital for both photoelectric efficiencies of various electronic devices and photocatalytic efficiency of different catalytic reactions.

To develop practical devices based on these coupled semiconductor nanoparticle systems, many efforts have been made to explore the possible CT process involved. Bessekhouad *et al.*[1] prepared CdS/TiO₂ and Bi₂S₃/TiO₂ heterojunctions with direct mixture and precipitation methods and analyzed the CT mechanism in the photocatalytic degradation of organic pollutants. Im *et al.*[2] used the bi-semiconductors of TiO₂ and

Fe₂O₃ as a photoelectrode material in a high performance dye-sensitized solar cell and discussed the mechanism whereby the conduction band of Fe₂O₃ works to prohibit the trapping effects of electrons in the conduction band of TiO₂. Ghadiri *et al.*[3] reported on the kinetics of the interfacial charge separation of PbS QDs/(001) TiO₂ nanosheets heterojunction solar cells. Additionally, MoS₂/TiO₂,[4] ZnO/TiO₂,[5] and ZnO/PbS,[6] heterojunctions were also investigated to study the charge-transfer processes in different applications. However, a research gap remains to be filled in order to reveal the CT processes in coupled semiconductor nanoparticle systems more intuitively, which calls for more suitable experimental techniques.

Since it was discovered on a rough silver electrode in 1974,[7] the surface-enhanced Raman scattering (SERS) has seen renewed interest over the past decades because of its high sensitivity, high selectivity, and nondestructive nature. Today SERS is being widely applied to many areas, such as analytical chemistry,[8–10] electrochemistry,[11] life science,[12–14] material area[15,16] and environment monitoring.[17] There are two primary mechanisms that account for SERS: electromagnetic mechanism (EM) and chemical enhancement mechanism (CM).[18,19] EM requires the coupling of metallic nanoparticles and incident radiation,[20] whereas CM involves a CT process between the substrate and adsorbate.[21,22] Typically, chemical enhancement is a resonance Raman-like process, which is sensitive to polarizability change of probe molecules. For most semiconductor materials, the surface plasmon resonant frequency is located in the infrared region. Thus, when semiconductor materials are applied as SERS substrates, the CM can be the dominant

[a]State Key Laboratory of Supramolecular Structure and Materials, Jilin University, Changchun 130012, P. R. China. E-mail: zhaob@mail.jlu.edu.cn; Fax: +86-431-85193421; Tel: +86-431-85168473

[b]Department of Electrical and Computer Engineering, Waterloo Institute for Nanotechnology (WIN), University of Waterloo, Waterloo, Ontario N2L 3G1, Canada

Paper

contribution to the surface-enhanced Raman signal on the semiconductor substrates, which provides an extensive space for studying CT processes in coupled semiconductor nanoparticle systems. That is to say, under the function of the chemical enhancement mechanism, the CT process in a definite system can be reflected in the corresponding SERS spectra by changing the polarizability of the adsorbed molecules. Therefore, one can study nanoscale interfacial CT processes in coupled semiconductor nanoparticle systems with the help of appropriate SERS CT models.

In this work, we fabricated an ordered coupled semiconductor nanoparticle system composed of TiO_2 NPs, probe molecules and PbS NPs as a SERS model to study the involved interfacial CT effects. The development of the semiconductor-coupled SERS model TiO_2/MBA/PbS was based on electrostatic interactions described in the literature with only slight modification.[23] First, the TiO_2 surfaces were first treated with MBA molecules where the –SH provides a binding site for Pb^{2+} ions. Then by reacting Na_2S with the Pb^{2+} ions, the PbS NPs were made onto the TiO_2 surfaces absorbed on the pretreated surfaces. Different from the method described previously, we replace the molecule mercaptopropionic acid (MPA) with MBA which functions as both a linker in coupled and a SERS probe to reveal how charge transits in our system. For MBA molecules, the carboxyl group and mercapto group can bind strongly to TiO_2 NPs and PbS NPs, respectively.[23,24] Thus, the order of this semiconductor-molecule-semiconductor CT system is fixed, which provides a high order for investigating the CT process. In this paper, the possible CT process involved in TiO_2/MBA/PbS is discussed to develop the theory behind interfacial CT effects between semiconductors. The present work is conducive to further investigation of the interfacial CT process in coupled semiconductor nanoparticle system with the SERS technique.

Experimental

Chemicals

4-Mercaptobenzoic acid (MBA) and titanium(IV) butoxide were purchased from Sigma-Aldrich and used without further purification. The other regents (lead nitrate, anhydrous ethanol, nitric acid, sodium sulfide) were all analytical grade. The distilled and deionized water from a Milli-Q-plus system with the resistivity >18.0 MΩ was used in aqueous solution.

Synthesis of TiO_2 NPs

In this work, the synthesis of TiO_2 NPs is mainly based on a sol–hydrothermal process described in previous literature.[22] First, a mixed solution of 5 mL of titanium(IV) butoxide and 5 mL of anhydrous ethanol was added dropwise into another mixed solution, consisting of 20 mL of anhydrous ethanol, 5 mL of deionized water, and 1 mL of 70% nitric acid, under rough stirring at room temperature. With the hydrolysis of titanium(IV) butoxide, a light yellow transparent sol was obtained by continuously stirring for 2 h. Then, the as-prepared sol was kept at 160 °C for 6 h in a stainless-steel vessel. After cooled to room temperature, the pasty production was washed with water and

dried at 60 °C for 24 h. Finally, TiO_2 NPs were obtained by calcining the dried product at 450 °C for 2 h.

Preparation of TiO_2/MBA system

The TiO_2/MBA system was prepared following the steps below. In brief, 20 mg of the prepared TiO_2 NPs was soaked in the MBA/ethanol solution (10^{-3} M) and the mixture was stirred for 6 h. Subsequently, the precipitate was centrifuged and rinsed with anhydrous ethanol once more. After drying, the TiO_2/MBA system was obtained.

Preparation of TiO_2/MBA/PbS system

The TiO_2/MBA/PbS system was prepared based on electrostatic interactions previously described in the literature with only slight modifications.[23,24] A 2 mM $Pb(NO_3)_2$ aqueous solution was added into the prepared TiO_2/MBA system to allow Pb^{2+} ions to absorb on the TiO_2 NP surfaces under stirring. To crystallize the PbS NPs onto the TiO_2, a 5 mM Na_2S aqueous solution was added. Then the pasty production was separated by centrifuge and washed with water. After drying at 60 °C for 24 h, we obtained the TiO_2/MBA/PbS system. The fabrication process of TiO_2/MBA/PbS system is presented in Fig. 1.

Preparation of TiO_2/MBA/CdS system

In order to preparing TiO_2/MBA/CdS system, we take advantage of the electrostatic interactions between nanoparticles and ions as previously described in the literature with only slight modifications.[25] A 2 mM $Cd(Ac)_2 \cdot 2H_2O$ ethanol solution was then added into the prepared TiO_2/MBA system to allow Cd^{2+} ions to absorb on the TiO_2 NP surfaces under stirring. To crystallize the CdS NPs onto the TiO_2 NPs, 6 mM thiourea was slowly added dropwise into the solution under vigorous stirring. Thereafter, the pH was adjusted to 10 with 0.2 M NaOH solution. Then the reaction was kept for an additional 12 h at room temperature. The resulting composite particles were washed with distilled water. After drying, the TiO_2/MBA/CdS system was obtained.

Instrumentation

TEM images were taken using a Jeol JEM 2100F transmission electron microscope operating at 200 kV. The crystal structure
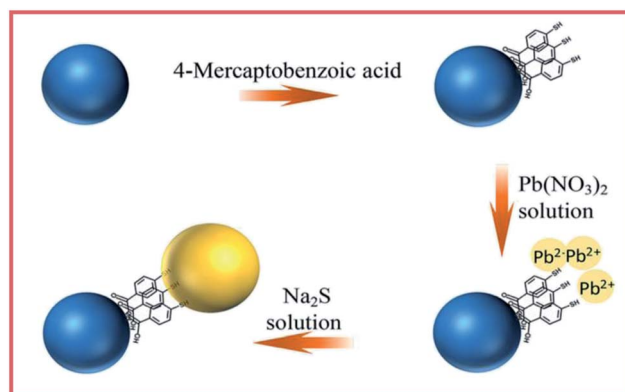

Fig. 1 The fabrication process of TiO_2/MBA/PbS system.

of samples was determined by X-ray diffraction (XRD) using a Siemens D5005 X-ray powder diffractometer with a Cu Kα radiation source at 40 kV and 30 mA. The ultraviolet-visible (UV-vis) diffuse reflectance spectra (UV-vis DRS) were recorded on a Lambda UV-950 UV-vis spectrometer. Raman spectra were obtained using a Horiba-Jobin Yvon LabRAM ARAMIS system. The 633 nm radiation from a 20 mW air-cooled HeNe narrow bandwidth laser was used as an exciting source. Data was acquired with the 10 s accumulations for MBA molecules in the different systems at ambient temperature. Meanwhile, to avoid the photodegradation effect, all the samples were tested with at a low laser power of 0.27 mW (monitored by filter D1).

Results and discussion

Characterization of morphology and crystal structure of different systems

Fig. 2a and b shows the TEM image and the X-ray diffraction (XRD) pattern of the TiO$_2$ NPs after hydrothermal processing and calcination. It can be seen from Fig. 2a that the TiO$_2$ NPs are all irregular sphere-like particles with a diameter of about 10 nm. According to JPCDS 21-1272, the observed lattice spacing of 0.351 nm in Fig. 2a corresponds to the (101) plane of

anatase TiO$_2$. Fig. 2b shows the XRD pattern of TiO$_2$ NPs calcined at 450 °C. In general, the XRD peak at $2\theta = 25.3°$ is identified as the characteristic diffraction peak of the anatase phase of TiO$_2$.[26]

Fig. 2b reveals that the TiO$_2$ NPs calcined at 450 °C were monolithic anatase phase TiO$_2$, which also agrees well with the reported data in JPCDS 21-1272. Estimated from the half-bandwidth (β) of the corresponding X-ray spectral peak by the Scherrer formula: $D = k\lambda/(\beta \cos\theta)$,[27] the crystalline size D was about 9.1 nm, which is consistent with the size value obtained from the TEM image.

Fig. 2c and d presents the TEM image and the XRD patterns of the TiO$_2$/MBA/PbS system. Inspection of the Fig. 2c TEM image reveals that PbS NPs, with an average diameter of about 70 nm, are surrounded by TiO$_2$ NPs. The crystallinity of PbS NPs can clearly be seen, where the distance of the crystalline plane was measured to be 0.342 nm, indicating a (111) plane of cubic PbS (JPCDS 05-0592). Fig. 2d shows the XRD pattern of the TiO$_2$/MBA/PbS system. The presence of PbS (black line, JPCD05-0592) and TiO$_2$ (red line, JPCDS 21-1272) diffraction peaks can be observed clearly in Fig. 2d. Both the TEM image and the XRD pattern provide clear evidence of the successful fabrication of the TiO$_2$/MBA/PbS system.
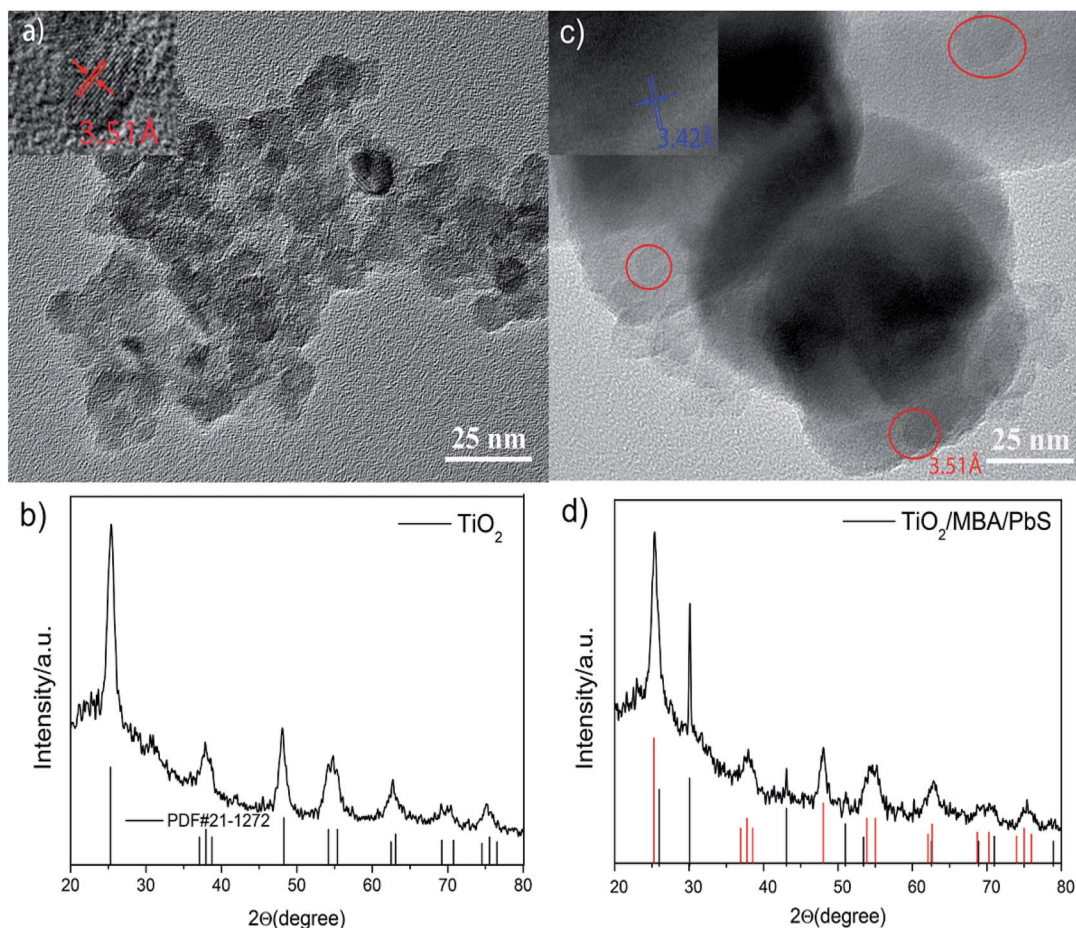

Fig. 2 The TEM image and the XRD patterns of the pure TiO$_2$ NPs (a and b) and TiO$_2$/MBA/PbS system (c and d). In (c), the particles inside red circle are TiO$_2$ NPs.
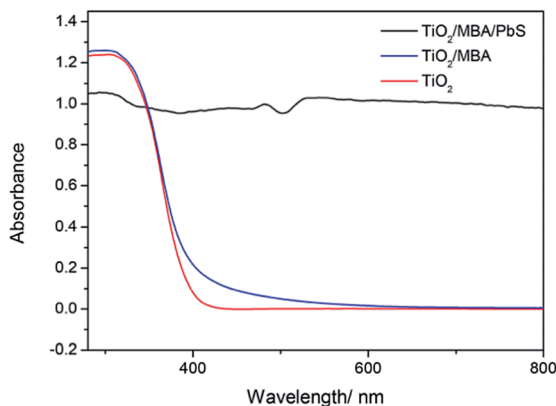
Fig. 3 The UV-visible absorption spectra have obtained to characterize the photoelectric property of different systems.

Measurement of UV-vis spectra

The UV-visible absorption spectra have obtained to characterize the photoelectric property of different systems. Fig. 3 shows the UV-vis absorption spectra of TiO_2, TiO_2/MBA and TiO_2/MBA/PbS systems. Pure TiO_2 shows a band-edge absorption around 395 nm (3.14 eV), which is close to the reported value.[28] After modification by MBA molecules, the photoabsorption threshold of TiO_2 exhibits a slight shift, which can be ascribed to the influence of the molecules adsorbed on TiO_2 NPs. Similar phenomena have been observed in previous literatures.[22,29,30] Moreover, its photoresponse is extended to about 600 nm. These changes can be attributed to a new charge-transfer (CT) complex formed between the adsorbed molecules and the TiO_2 substrate. After introducing PbS NPs, the system shows a strong absorption of visible light because of PbS NPs presence. By comparison, we also synthesize cubic PbS NPs with similar diameter of about 70 nm (Fig. S1†). Fig. S2† shows the UV-vis absorption spectra of PbS NPs with strong absorption between 200–800 nm. Thus, it can be concluded that the TiO_2/MBA/PbS coupled semiconductor nanoparticle system is fabricated.

SERS spectra of different semiconductor systems

SERS spectra (excited at 633 nm) of MBA molecules in the TiO_2/MBA and TiO_2/MBA/PbS systems are shown in Fig. 4a.

To avoid the photodegradation effect of laser, all the samples were tested at a low laser power of 0.27 mW (monitored by filter D1).[31] The Raman shifts and assignments of the bands are listed in Table 1.

For MBA molecules in the TiO_2/MBA system (black line, Fig. 4a), one of the predominant bands is located at 1075 cm^{-1}, which has been assigned to the in-plane ring breathing mode coupled with ν(C–S). Another predominant band is an overlap result of two SERS bands: the aromatic ν(CC) mode (at 1592 cm^{-1}) and the non-totally symmetric stretching mode (at 1583 cm^{-1}).[32,33] Two weak bands at about 1147 (ν15, b2) and 1181 cm^{-1} (ν9, a1) can also be observed and are attributed to the C–H deformation mode. These two weak bands are characteristic SERS signals of the 4-MBA molecule on the TiO_2 substrates and consistent with those previously reported in TiO_2/4-MBA
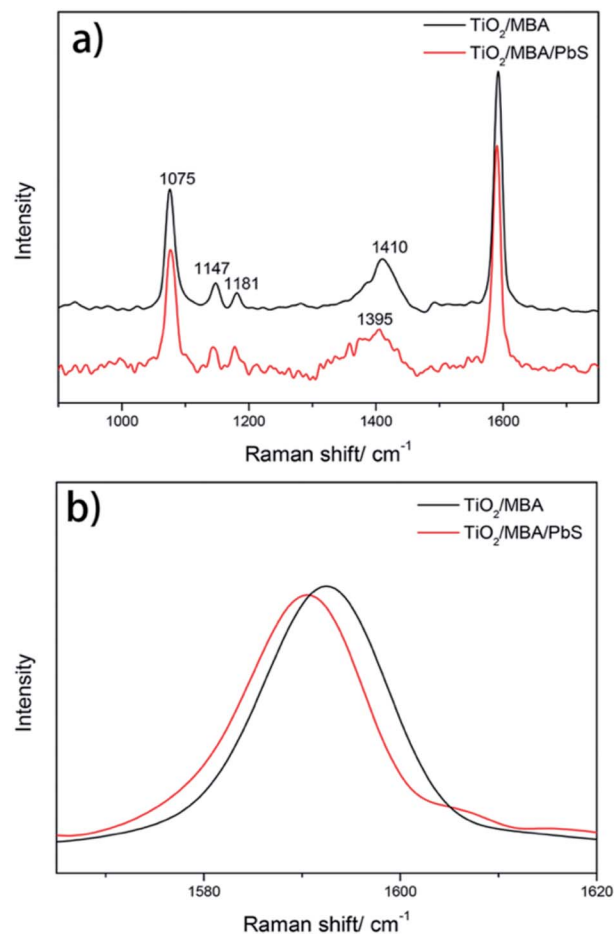

Fig. 4 (a) The SERS spectra of TiO_2/MBA and TiO_2/MBA/PbS systems at 633 nm excitation and (b) the enlarged SERS spectra between 1565 and 1620 cm^{-1}.

systems. In previous works,[30,34] the SERS signals in the TiO_2/MBA system have been attributed to the dominant contribution of the TiO_2-to-molecule CT mechanism. After introducing PbS NPs into the TiO_2/MBA system (black line, Fig. 4a), some changes in the SERS bands were observed. For comparison, the Raman spectra were normalized using the band at 1075 cm^{-1}. For clarity, the magnified SERS spectra of 4-MBA molecules

Table 1 Wavenumbers and assignments of bands in the SERS spectrum of MBA molecular[a]

Wavenumbers (cm^{-1})	Band assignments
1075	In-plane ring breathing + ν(C–S)
1147	C–H deformation modes ν15, b2
1181	C–H deformation modes ν9, a1
1411	β(O–H) + ν(C-ph) + 19a + ν(CO$_2$), b2
1583	Non-totally symmetric ν(CC), b2
1592	Totally symmetric ν(CC), a1

[a] ν, stretching; β, bending. For ring vibrations, the corresponding vibrational modes of benzene and the symmetry species with C_{2v} symmetry are indicated.
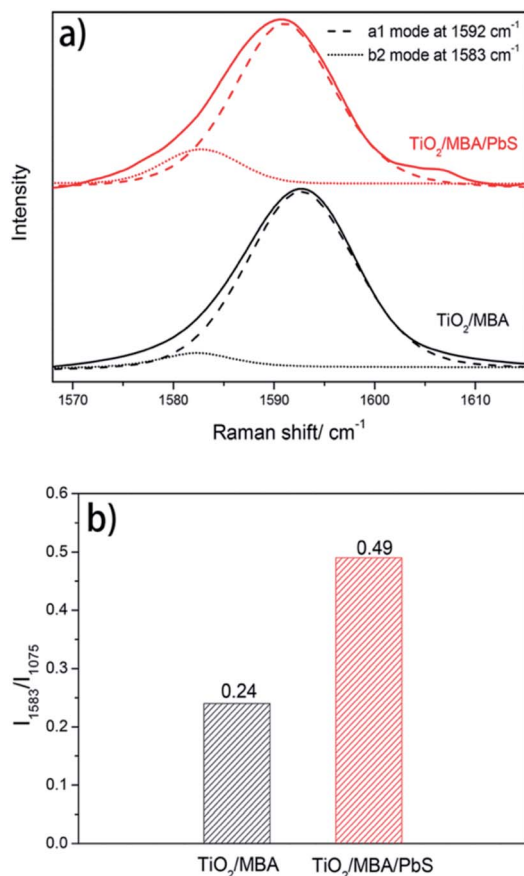
Fig. 5 (a) The nonlinear Lorentzian fit curve of the SERS spectra in the TiO$_2$/MBA and TiO$_2$/MBA/PbS systems between 1568 and 1615 cm^{-1}; (b) the SERS intensity ratio between the modes at 1583 and 1075 cm^{-1} spectra in the TiO$_2$/MBA and TiO$_2$/MBA/PbS systems.

between 1565 and 1620 cm^{-1} are shown in Fig. 4b. The band at 1583 cm^{-1} assigned to non-totally symmetric ν(CC) displays an increase in the intensity of the SERS spectrum after introducing PbS NPs, while band at 1592 cm^{-1} assigned to the aromatic ν(CC) mode has no distinct changes. Meanwhile, it is worth noting that the peak at 1410 cm^{-1} (Fig. 4a) is broadened and shifts after the introduction of PbS NPs, which provides more evidence that MBA molecules bind to TiO$_2$ and PbS with COO$^-$ and –SH respectively (shown in ESI†). According to the previous report,[35] the composite peak at 1411 cm^{-1}, rising from the combination or overlap of O–H bending, the carboxyl carbon and aromatic carbon stretching, 19a (the Wilson notation) coupled with COO$^-$ asymmetric stretch, can be ascribed to b2 mode. Thus, due to the selective enhancement of b2 mode, the increased peak area at 1411 cm^{-1} is observed after the introduction of PbS NPs.

According to the CT model of Lombardi,[21] only totally symmetric vibrational modes of the probe molecules are expected to be enhanced via the Franck–Condon contribution, and the Herzberg–Teller effect can enhance both totally and non-totally symmetric vibrational signatures in the SERS spectra of the probe molecules. That is, the b2 mode can be selectively enhanced by the CT mechanism through the Herzberg–Teller

contribution. To further demonstrate the enhancement of b2 mode in the TiO$_2$/MBA/PbS system, the nonlinear Lorentzian curve fit of the SERS spectra was performed. In Fig. 5a, an enhancement of the b2 mode in SERS spectra of MBA molecules is observed in the fit result. For comparison, we also calculated the intensity ratio between the two modes at 1583 cm^{-1} (b2) and 1075 cm^{-1} (a1) and plotted the column diagram (Fig. 5b). The band at 1075 cm^{-1} (C–S stretch, a1) was selected because it is intense and relatively isolated from interference. The fit result indicates that the b2 mode is enhanced selectively derived from the enhanced CT process that occurs after introducing PbS NPs into the TiO$_2$/MBA system. As we know, the SERS signals in TiO$_2$/MBA have been attributed to the dominant contribution of the TiO$_2$-to-molecule CT mechanism.[22,34,36] Then, it can be deduced that the introduction of PbS NPs enhances the TiO$_2$-to-molecule CT process. These results agree with previous reports of the SERS spectra of MBA.[33] Additionally, Fig. S3 in the ESI† shows the SERS spectrum of the PbS/MBA system, which further prove that the changes in SERS occur due to the interaction between TiO$_2$ NPs and PbS NPs.

It is also noteworthy that the interaction in TiO$_2$/MBA/PbS system also influences the phonon vibrational mode of TiO$_2$ NPs. Fig. 6 shows the Raman spectra of TiO$_2$ collected from TiO$_2$/MBA and TiO$_2$/MBA/PbS systems in the region of 100–700 cm^{-1}. Raman modes at 145, 197, 398, 517 and 639 cm^{-1} are assigned as

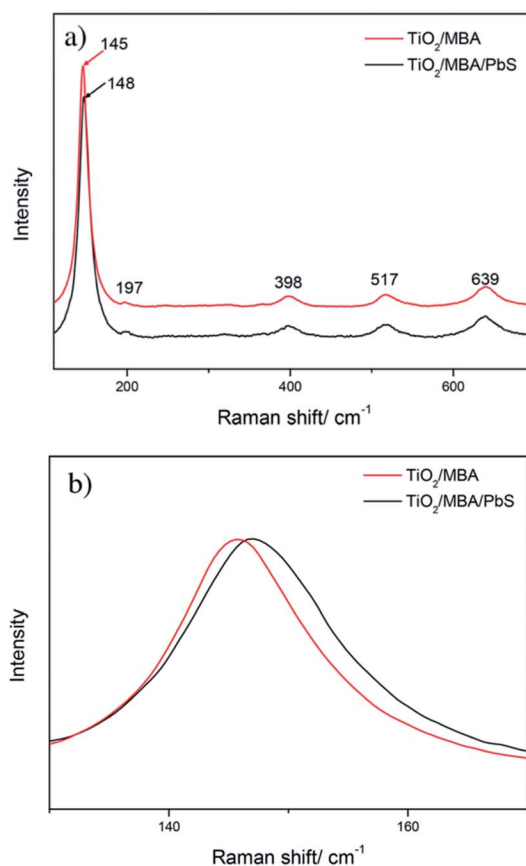**Fig. 6** (a) The Raman spectra of TiO$_2$ collected from TiO$_2$/MBA and TiO$_2$/MBA/PbS systems in the region of 100–700 cm^{-1} and (b) the enlarged SERS spectra between 130 and 170 cm^{-1}.

Eg, Eg, B1g, A1g (or B1g), and Eg modes in anatase phase, respectively.[37] For comparison, they are also normalized to the intensity of the Eg(1) peak (145 cm^{-1} in TiO$_2$/MBA). It can be observed that the peak at 145 cm^{-1} shifts toward higher wavenumbers and broadens after introducing PbS NPs into TiO$_2$/MBA (Fig. 6b). As Fig. 4S† shows, the changes in TiO$_2$/MBA/PbS come from the interaction between TiO$_2$ and PbS, instead of MBA molecules. Thus, it can be deduced that the introduction of PbS NPs enhanced the CT process from TiO$_2$ to MBA molecules, which further influences the phonon density of states in anatase TiO$_2$. Then, the changes are reflected in the Raman spectra of TiO$_2$ phonon vibrational mode. This phenomenon is similar to previous work where the light-induced transformations were observed due to the interaction between the TiO$_2$ and Au NPs.[38]

Analysis of the CT effect in the TiO$_2$/MBA/PbS system

As Fig. 5 shows, the intensity of the SERS signal at 158 cm^{-1} (b2), driven by the enhancement of the TiO$_2$-to-molecule CT process in TiO$_2$/MBA/PbS system, is obviously higher than that in the TiO$_2$/MBA system. According to previous work, in TiO$_2$/

MBA/Ag sandwich-structure system the stronger electrons attracting ability of Ag NPs promotes the TiO$_2$-to-molecule CT process. In this work, it seems that the PbS NPs in TiO$_2$/MBA/PbS system possibly play a similar role in the TiO$_2$-to-molecule CT process. In previous work,[23,39] efficient electron transfer from PbS QDs to TiO$_2$ occurs only for QD diameters below approximately 4.3 nm. However, as Fig. 2c shows, the diameter of PbS NPs in our system is about 70 nm. And the work function of PbS NPs is 4.9 eV, which is higher than that of TiO$_2$ NPs (4.7 eV).[40,41] As the two kinds of materials with different work functions come in close contact with each other, the electrons are driven to transfer from one with lower work function to the other until equilibration of Fermi level. Therefore, when TiO$_2$ NPs come into contact with PbS NPs in the TiO$_2$/MBA/PbS system, electrons tend to transit from TiO$_2$ to PbS, which is favorable to TiO$_2$-to-molecule CT process. Then, the enhancement of b2-type vibrational mode is observed in SERS spectra (Fig. 5a). Similar phenomenon where the SERS spectra changes due to the interaction of two kinds of semiconductor NPs has been reported by Qian et al. previously.[25] In their report, the SERS signal of bridge molecules show similar
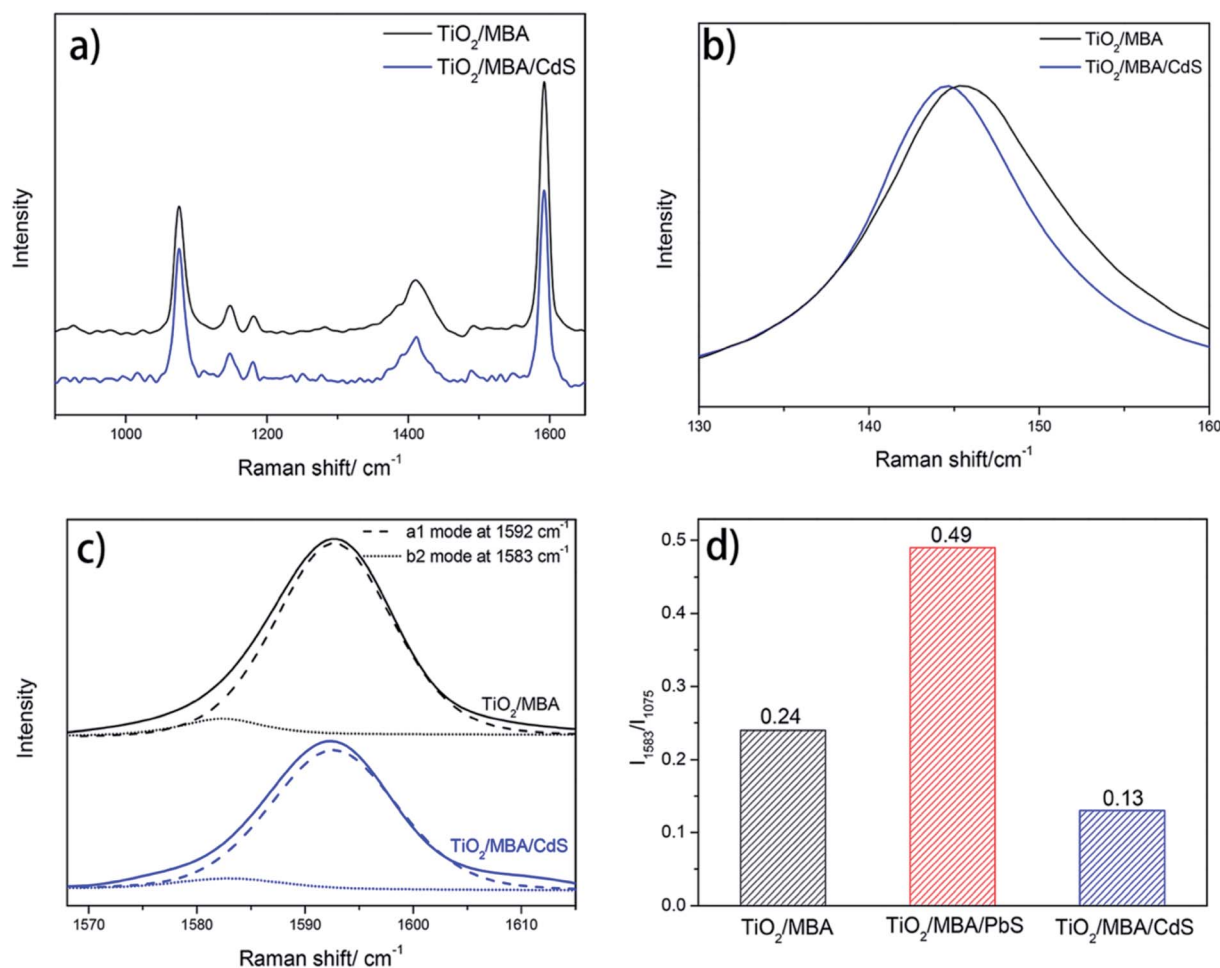

Fig. 7 (a) The SERS spectra of the TiO$_2$/MBA and TiO$_2$/MBA/CdS systems at 633 excitation, and (b) the enlarged SERS spectra between 1560 and 1620 cm^{-1}; (b) the enlarged SERS spectra between 130 and 170 cm^{-1}; (c) the nonlinear Lorentzian curve fit of the SERS spectra in TiO$_2$/MBA and TiO$_2$/MBA/CdS systems between 1568 and 1615 cm^{-1}, and (d) the SERS intensity ratio between the modes at 1583 and 1075 cm^{-1} in the TiO$_2$/MBA, TiO$_2$/MBA/PbS and TiO$_2$/MBA/CdS systems.

changes after introducing CdS NPs into the TiO_2/MPA system. From the above discussion, it can be deduced that the interaction between the semiconductor NPs has an effect on the TiO_2-to-molecule CT process. And the effect can be reflected in the SERS spectra where the CT-sensitive bands show enhancement under the interaction. Thus, the SERS model of the "donor–bridge–acceptor" system may be applicable to investigate the interfacial CT effect between different materials.

SERS spectra of the TiO_2/MBA/CdS system

To further confirm the proposed mechanism, we also investigated the SERS spectra of the TiO_2/MBA/CdS system in Fig. 7. The XRD pattern and TEM of the TiO_2/MBA/CdS system are shown in Fig. S5.† The work function of CdS NPs is 4.5 eV, which is lower than that of TiO_2 NPs (4.7 eV).[40,41] Therefore, when TiO_2 NPs come in contact with CdS NPs in the TiO_2/MBA/CdS system, electrons tend to transit from CdS NPs to TiO_2, which is consistent with previous works. Then the TiO_2-to-molecule CT process is inhibited. As we expect, the SERS spectra of the TiO_2/MBA/CdS system would show opposite changes compared with the TiO_2/MBA/PbS system. Fig. 7a shows the SERS spectra (excited at 633 nm) of MBA molecules in the TiO_2/MBA and TiO_2/MBA/CdS systems. For comparison, the

Raman spectra were also normalized using the band at 1075 cm^{-1}. After introducing CdS NPs, the band at 1583 cm^{-1} assigned to non-totally symmetric ν(CC) displays a decrease in the intensity of the SERS spectrum, while the band at 1592 cm^{-1} assigned to the aromatic ν(CC) mode shows no significate changes (Fig. 7c and d). The SERS spectrum of CdS/MBA is shown in Fig. S6† to exclude the interference from CdS/MBA.

Meanwhile, the Raman spectra of TiO_2 collected in the TiO_2/MBA/CdS system also show opposite changes compared with the TiO_2/MBA/PbS system. As Fig. 8 shows, the peak at 145 cm^{-1} shifts toward lower wavenumber and becomes narrower after introducing CdS NPs into TiO_2/MBA, which is completely opposite to what we observed in the TiO_2/MBA/PbS system.

From above analysis, it can be deduced that the CT process between different semiconductor NPs has different effects on the TiO_2-to-molecule CT process. And these effects on the TiO_2-to-molecule CT process can be reflected in the SERS spectra where the CT-sensitive vibrational modes of probe molecules and the phonon vibrational mode of TiO_2 show different changes. Thus, the CT process in coupled semiconductor nanoparticle systems can be investigated by applying the SERS method to a semiconductor-probe molecule-semiconductor physical model.

Conclusions

In this work, the TiO_2/MBA/PbS system has been fabricated as a model to study the interfacial CT effects in coupled semiconductor nanoparticle system with SERS technique. As compared with the SERS signal in the TiO_2/MBA system, the SERS signals of MBA in the TiO_2/MBA/PbS system show distinct differences. The peak assigned to the b2 mode is significantly enhanced in the TiO_2/MBA/PbS system. Meanwhile, the Raman spectra of TiO_2 phonon vibrational mode also exhibit obvious difference in Raman frequency. These phenomena can be ascribed to the interaction between the TiO_2 and PbS NPs where the CT trend from TiO_2 to molecules is enhanced because the Fermi level of TiO_2 is higher than that of PbS NPs. To prove this point, we also investigated SERS spectra of the TiO_2/MBA/CdS system where the relative position of Fermi level is different from that of the TiO_2/MBA/PbS system. And the result is in good accordance with our proposed mechanism. Thus, we can conclude from this work that it is possible to investigate the CT process in coupled semiconductor nanoparticle systems with a semiconductor–bridge molecule–semiconductor physical SERS model. It is expected that this study will not only provide a deep investigation of the CT process in coupled semiconductor nanoparticle systems but also be valuable for practical application of SERS technology in the nanomaterial field.

Conflicts of interest

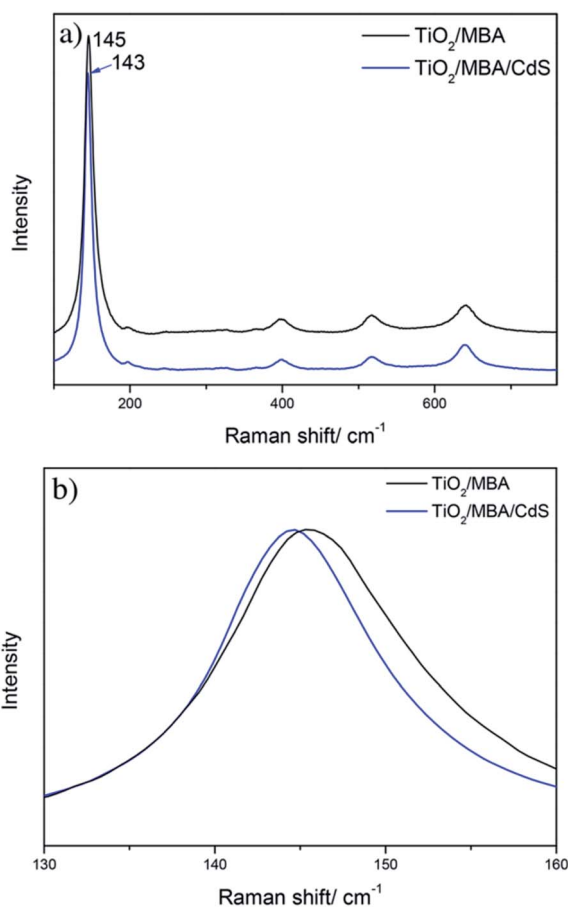There are no conflicts to declare.

Acknowledgements

Fig. 8 (a) The Raman spectra of TiO_2 collected from the TiO_2/MBA and TiO_2/MBA/CdS systems, and (b) the enlarged SERS spectra between 130 and 160 cm^{-1}.

References

1 Y. Bessekhouad, D. Robert and J. V. Weber, *J. Photochem. Photobiol., A*, 2004, **163**, 569–580.

2 J. S. Im, S. K. Lee and Y.-S. Lee, *Appl. Surf. Sci.*, 2011, **257**, 2164–2169.

3 E. Ghadiri, B. Liu, J.-E. Moser, M. Grätzel and L. Etgar, *Part. Part. Syst. Charact.*, 2015, **32**, 483–488.

4 Z. He, W. Que, Y. Xing and X. Liu, *J. Alloys Compd.*, 2016, **672**, 481–488.

5 S. A. Mozaffari, M. Ranjbar, E. Kouhestanian, H. Salar Amoli and M. H. Armanmehr, *Mater. Sci. Semicond. Process.*, 2015, **40**, 285–292.

6 S. Sardar, P. Kar, S. Sarkar, P. Lemmens and S. K. Pal, *Sol. Energy Mater. Sol. Cells*, 2015, **134**, 400–406.

7 M. Fleischmann, P. J. Hendra and A. J. McQuillan, *Chem. Phys. Lett.*, 1974, **26**, 163–166.

8 R. P. Li, J. L. Yang, J. H. Han, J. H. Liu and M. J. Huang, *Phys. E*, 2017, **88**, 164–168.

9 C. Y. Zhang, R. Hao, B. Zhao, Y. Z. Fu, H. J. Zhang, S. Moeendarbari, C. S. Pickering, Y. W. Hao and Y. Q. Liu, *Appl. Surf. Sci.*, 2017, **400**, 49–56.

10 X. G. Zhang, Z. G. Dai, S. Y. Si, X. L. Zhang, W. Wu, H. B. Deng, F. B. Wang, X. H. Xiao and C. Z. Jiang, *Small*, 2017, **13**, 1603347.

11 R. Berenguer, A. La Rosa-Toro, C. Quijada and E. Morallon, *Appl. Catal., B*, 2017, **207**, 286–296.

12 C. C. Lin, C. Y. Lin, C. J. Kao and C. H. Hung, *Sens. Actuators, B*, 2017, **241**, 513–521.

13 K. K. Reza, J. Wang, R. Vaidyanathan, S. Dey, Y. L. Wang and M. Trau, *Small*, 2017, **13**, 1602902.

14 Y. Sun, L. Xu, F. D. Zhang, Z. G. Song, Y. W. Hu, Y. J. Ji, J. Y. Shen, B. Li, H. Z. Lu and H. F. Yang, *Biosens. Bioelectron.*, 2017, **89**, 906–912.

15 X. M. Li, M. H. Bi, L. Cui, Y. Z. Zhou, X. W. Du, S. Z. Qiao and J. Yang, *Adv. Funct. Mater.*, 2017, **27**, 1605703.

16 A. K. Pal and D. B. Mohan, *J. Alloys Compd.*, 2017, **698**, 460–468.

17 S. G. Harroun, Y. T. Zhang, T. H. Chen, C. R. Ku and H. T. Chang, *Spectrochim. Acta, Part A*, 2017, **176**, 1–7.

18 A. Campion and P. Kambhampati, *Chem. Soc. Rev.*, 1998, **27**, 241–250.

19 R. S. Das and Y. K. Agrawal, *Vib. Spectrosc.*, 2011, **57**, 163–176.

20 E. J. Zeman and G. C. Schatz, *J. Phys. Chem.*, 1987, **91**, 634–643.

21 J. R. Lombardi and R. L. Birke, *J. Phys. Chem. C*, 2008, **112**, 5605–5617.

22 L. Yang, X. Jiang, W. Ruan, B. Zhao, W. Xu and J. R. Lombardi, *J. Phys. Chem. C*, 2008, **112**, 20095–20098.

23 C. Ratanatawanate, C. Xiong and K. J. Balkus, *ACS Nano*, 2008, **2**, 1682–1688.

24 Y. Sun, E. Hao, X. Zhang, B. Yang, M. Gao and J. Shen, *Chem. Commun.*, 1996, 2381–2382, DOI: 10.1039/CC9960002381.

25 S. Qian, C. Wang, W. Liu, Y. Zhu, W. Yao and X. Lu, *J. Mater. Chem.*, 2011, **21**, 4945–4952.

26 X. Xue, W. Ji, Z. Mao, Z. Li, W. Ruan, B. Zhao and J. R. Lombardi, *Spectrochim. Acta, Part A*, 2012, **95**, 213–217.

27 W. Choi, A. Termin and M. R. Hoffmann, *J. Phys. Chem.*, 1994, **98**, 13669–13679.

28 L. B. Liao, H. Y. Zhou and X. M. Xiao, *Chem. Phys.*, 2005, **316**, 164–170.

29 X. Xue, W. Ji, Z. Mao, H. Mao, Y. Wang, X. Wang, W. Ruan, B. Zhao and J. R. Lombardi, *J. Phys. Chem. C*, 2012, **116**, 8792–8797.

30 L. Yang, X. Jiang, W. Ruan, J. Yang, B. Zhao, W. Xu and J. R. Lombardi, *J. Phys. Chem. C*, 2009, **113**, 16226–16231.

31 P. Yin, R. U. I. Zhang, Y. Zhang and L. I. N. Guo, *Int. J. Mod. Phys. B*, 2010, **24**, 3257–3262.

32 X. Zhang, Z. Yu, W. Ji, H. Sui, Q. Cong, X. Wang and B. Zhao, *J. Phys. Chem. C*, 2015, **119**, 22439–22444.

33 Y. Wang, W. Ji, H. Sui, Y. Kitahama, W. Ruan, Y. Ozaki and B. Zhao, *J. Phys. Chem. C*, 2014, **118**, 10191–10197.

34 X. Jiang, X. Li, X. Jia, G. Li, X. Wang, G. Wang, Z. Li, L. Yang and B. Zhao, *J. Phys. Chem. C*, 2012, **116**, 14650–14655.

35 R. Li, H. Lv, X. Zhang, P. Liu, L. Chen, J. Cheng and B. Zhao, *Spectrochim. Acta, Part A*, 2015, **148**, 369–374.

36 L. Yang, Y. Zhang, W. Ruan, B. Zhao, W. Xu and J. R. Lombardi, *J. Raman Spectrosc.*, 2009, 721–726, DOI: 10.1002/jrs.2511.

37 S. Kelly, F. H. Pollak and M. Tomkiewicz, *J. Phys. Chem. B*, 1997, **101**, 2730–2734.

38 O. L. Stroyuk, V. M. Dzhagan, A. V. Kozytskiy, A. Y. Breslavskiy, S. Y. Kuchmiy, A. Villabona and D. R. T. Zahn, *Mater. Sci. Semicond. Process.*, 2015, **37**, 3–8.

39 D. F. Wang, H. G. Zhao, N. Q. Wu, M. A. El Khakani and D. L. Ma, *J. Phys. Chem. Lett.*, 2010, **1**, 1030–1035.

40 K. P. Bhandari, P. J. Roland, H. Mahabaduge, N. O. Haugen, C. R. Grice, S. Jeong, T. Dykstra, J. Gao and R. J. Ellingson, *Sol. Energy Mater. Sol. Cells*, 2013, **117**, 476–482.

41 A. R. Kumarasinghe, W. R. Flavell, A. G. Thomas, A. K. Mallick, D. Tsoutsou, C. Chatwin, S. Rayner, P. Kirkham, S. Warren, S. Patel, P. Christian, P. O'Brien, M. Gratzel and R. Hengerer, *J. Chem. Phys.*, 2007, **127**, 114703.